Neutrino detection and Detector analysis

Akshay Shankar

July 26, 2019

Contents

1 Introduction

1.1 Neutrino Physics

The existence of neutrinos in nature was first postulated in 1930 by Pauli to explain the apparent violation of energy conservation in nuclear beta decays.

$$n \rightarrow p^+ + e^- + \bar{\nu}_e$$

The resultant electron was observed to have a range of energies instead of the expected full reaction energy. To explain this, Pauli suggested the formation of a light, neutral particle besides the neutron and this particle was named the 'neutrino' and was experimentally observed 23 years later, in a reactor experiment performed by C.Cowan and F.Reines.

In the next few decades, it was observed that neutrinos existed in three different flavour species; ν_e, ν_μ, ν_τ. The nature of ν_e and ν_μ neutrinos were demonstrated in 1962 in an accelerator neutrino experiment at Brookhaven National Laboratory, and the ν_τ was demonstrated in 2000 at Fermilab.
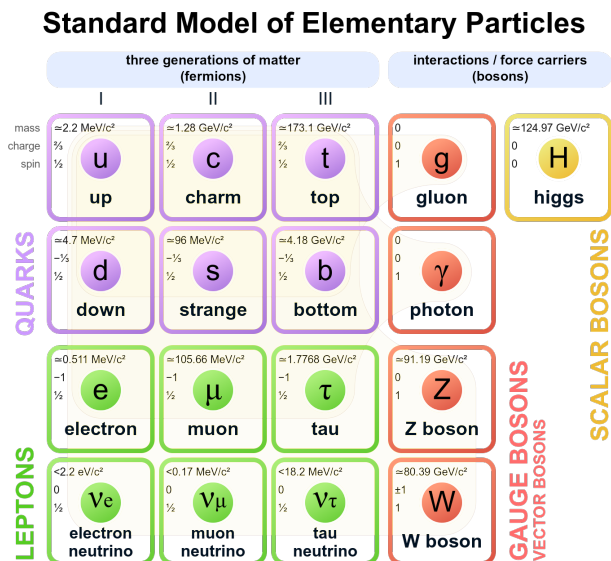
Figure 1.1: The Standard Model

Neutrinos are fundamental constituents of matter and are assumed to be massless fermions in the Standard Model of fundamental particles. The Standard Model comprises of 6 quarks and 6 leptons along with their anti-particles and 4 mediators as shown in figure 1.1. Each charged lepton (e, μ, τ) has a corresponding neutrino in the Standard Model. Since neutrinos carry no charge and have a tiny mass, they interact with matter only through the weak force due to which they are difficult to detect.

Figure 1.2: Various sources of neutrinos

As seen in fig 1.2, neutrinos can be observed at a wide range of energies. There are three major sources of neutrinos;

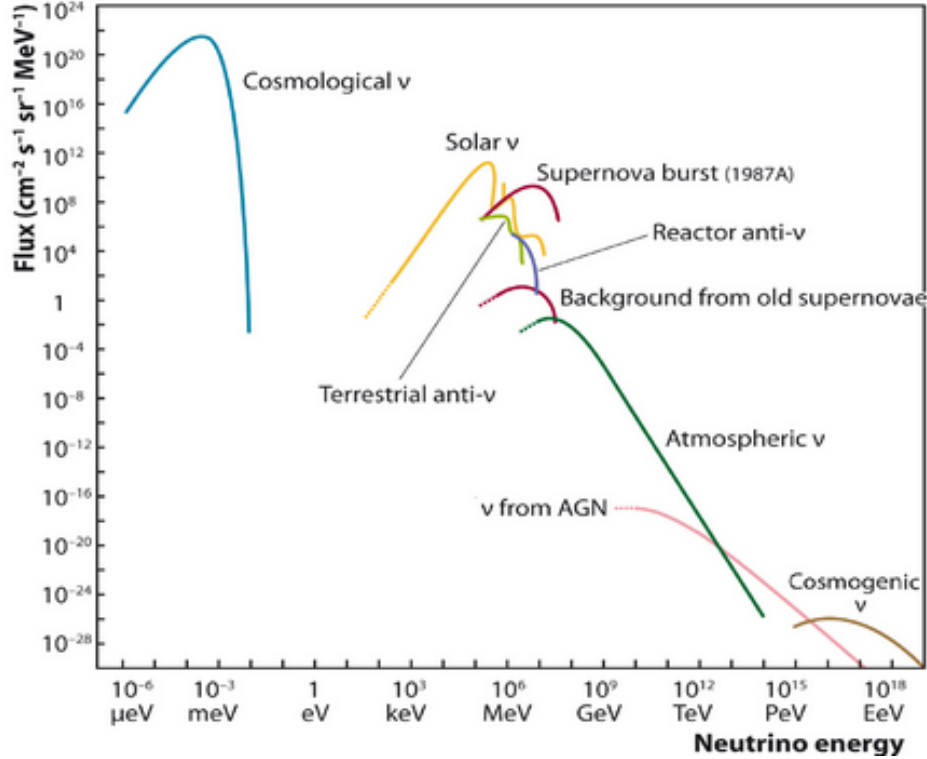- **Atmospheric neutrinos:** The interaction of cosmic rays with upper layers of the atmosphere produces various mesons (like π, K) that further cascade, resulting in neutrino production along with other particles. They are mostly muon neutrinos.

- **Solar neutrinos:** As a result of the thermonuclear fusion reactions in the sun, neutrinos are produced. These neutrinos are used to model the heat signatures of the sun, as neutrinos escape the sun easier than light due to their weak interactions. They are mostly electron neutrinos.

- **Reactor/Accelerator neutrinos**: When protons are accelerated to nearly the speed of light and collided against each other, it produces pions and kaons which decay to produce high energy neutrinos. Fission reactions in nuclear plants also result in neutrino production.

As neutrinos are weakly interacting particles, they tend to travel large distances without being interrupted. During this travel, the neutrino can change from one flavour to another due to a phenomenon known as **"neutrino oscillation"**. This was first observed when the flux of electron neutrinos from the sun was observed to be lesser than expected. It was later found out that a lot of the electron neutrinos oscillated to muon and tau neutrinos before it reached the detectors on earth. The next section elaborates on this phenomenon.

1.2 Neutrino Oscillation

The experiments with solar, atmospheric and reactor neutrinos have provided evidences for oscillations of neutrinos caused by nonzero neutrino masses and neutrino mixing. It was found out that neutrinos exist in flavour eigenstates $(\nu_e, \nu_\mu, \nu_\tau)$ while interacting with matter, and in mass eigenstates (ν_1, ν_2, ν_3) while propagating. The three neutrino flavour eigenstates are superpositions of the mass eigenstates and are related by a 3x3 unitary matrix known as the **Maki-Nakagawa-Sakata (MNS) matrix**. The relationship can be expressed by the following matrix equation:

$$\begin{pmatrix} \nu_e \\ \nu_\mu \\ \nu_\tau \end{pmatrix} = \begin{pmatrix} U_{e1} & U_{e2} & U_{e3} \\ U_{\mu1} & U_{\mu2} & U_{\mu3} \\ U_{\tau1} & U_{\tau2} & U_{\tau3} \end{pmatrix} \begin{pmatrix} \nu_1 \\ \nu_2 \\ \nu_3 \end{pmatrix}$$

The 3x3 MNS matrix can be expressed as:

$$U = \begin{pmatrix} 1 & 0 & 0 \\ 0 & cos(\theta_{23}) & sin(\theta_{23}) \\ 0 & -sin(\theta_{23}) & cos(\theta_{23}) \end{pmatrix} \begin{pmatrix} cos(\theta_{13}) & 0 & sin(\theta_{13})e^{i\delta} \\ 0 & 1 & 0 \\ -sin(\theta_{13})e^{i\delta} & 0 & cos(\theta_{13}) \end{pmatrix} \begin{pmatrix} cos(\theta_{12}) & sin(\theta_{12}) & 0 \\ -sin(\theta_{12}) & cos(\theta_{12}) & 0 \\ 0 & 0 & 1 \end{pmatrix}$$

where θ_{12}, θ_{23} and θ_{13} are the mixing angles and δ is the CP violating phase.

With three neutrino masses, there are two neutrino mass differences($\Delta m_{21}^2, \Delta m_{32}^2$) along with the three mixing angles and one CP violating phase. Neutrino oscillation was discovered by the Super-Kamiokande experiment in 1998, as the number of up-going atmospheric neutrinos were observed to be nearly half of the number of down-going ones, as muon neutrinos passing through the earth have a higher probability of turning into tau neutrinos.
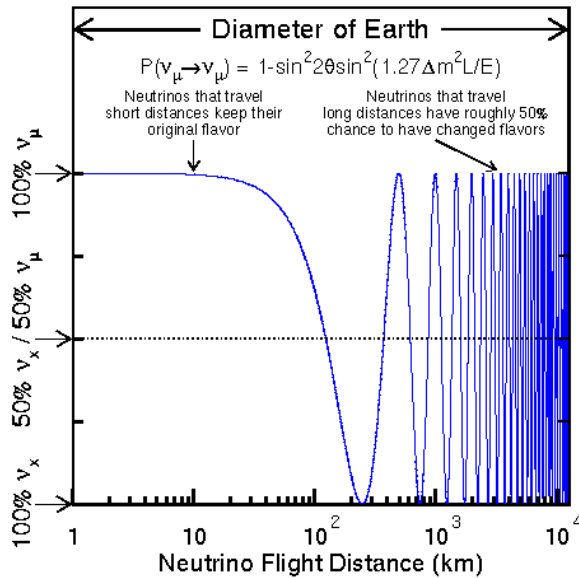

Figure 1.3: Probability of neutrino oscillation occurring while propagating through the earth

3

Currently, the values of the two mass squared differences and two mixing angles $(\theta_{23}, \theta_{12})$ are known from other experiments. The disappearance of solar neutrinos (ν_e) is driven by the oscillations of 1-2 mass states, which are mixed by the matrix with θ_{12} terms, and the disappearance of the atmospheric neutrinos (ν_μ) is driven by the matrix having θ_{23} terms. In the middle mixing matrix, the θ_{13} term is unmeasured and its non-zero value is a high priority topic in neutrino physics.
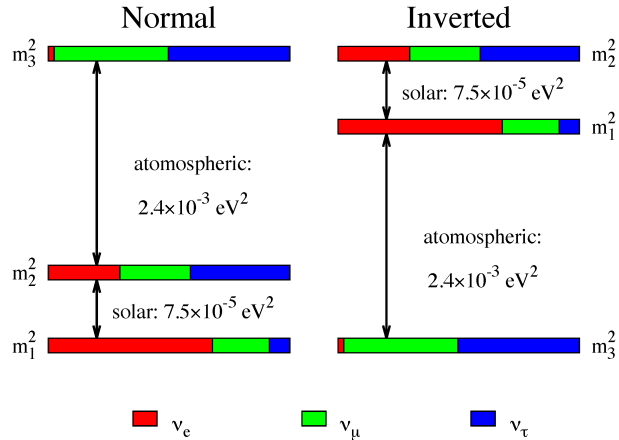

Figure 1.4: Normal and Inverted mass heirarchy

The pattern of neutrino masses are only partially known. The solar neutrino experiments have helped us infer the sign of Δm_{21}^2 because the matter effect (MSW effect) in the sun results in more solar neutrino oscillations and this effect depends on the sign of the mass squared term. However, the atmospheric neutrino data do not have significant sensitivity to matter effects, due to which it is not determined whether $m_2 < m_3$ or $m_2 > m_3$. Due to this ambiguity in the neutrino masses, there exist two possible mass heirarchies;

- **Normal heirarchy:** $m_1 < m_2 < m_3$

- **Inverted heirarchy:** $m_3 < m_1 < m_2$

The mass heirarchy problem is also a high priority topic in neutrino physics and several long baseline experiments have been planned in order to determine the sign of the mass squared term, such as Hyper Kamiokande and INO-ICAL.

1.3 Oscillations in Matter

The probability of a ν_a neutrino turning into a ν_b neutrino in vacuum is given by:

$$P_{(\nu_a \to \nu_b)} = \delta_{ab} - 4 \sum_{j>i} Re(U_{ai}^* U_{bi} U_{aj} U_{bj}^*) sin^2(1.27 \Delta m_{ij}^2 \frac{L}{E}) \pm 2 \sum_{j>i} Im(U_{ai}^* U_{bi} U_{aj} U_{bj}^*) sin^2(2.54 \Delta m_{ij}^2 \frac{L}{E}).$$

where L is distance travelled in km, E is energy of the neutrino in GeV, Δm_{ij}^2 is the mass squared difference in eV^2, and U_{ij} are the elements of the MNS matrix.

However, when neutrinos pass through matter, it influences the neutrino propagation due to which the oscillation probability in presence of matter will be different when compared to the probability in vacuum. Neutrinos can interact with matter via the weak force in the following two ways:

1.3.1 Charged Current interactions

The interaction is called 'charged' because the charged W boson is the mediator in the weak interaction of the neutrino with matter.
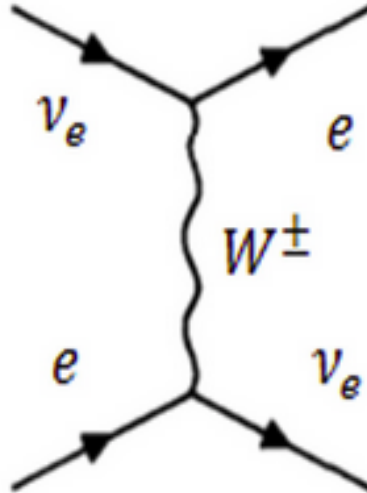

Figure 1.3: Feynman diagram of charged current interaction

This interaction results in changing the flavour of the quark and changing the neutrino to its corresponding charged lepton.

$$X + \nu_l \to Y + l^-$$
$$X + \bar{\nu}_l \to Y + l^+$$

[X,Y - Hadrons; l - lepton; ν_l - neutrino]

1.3.2 Neutral Current interactions

The interaction is called 'neutral' because the neutral Z boson is the mediator in the weak interaction of the neutrino with matter.
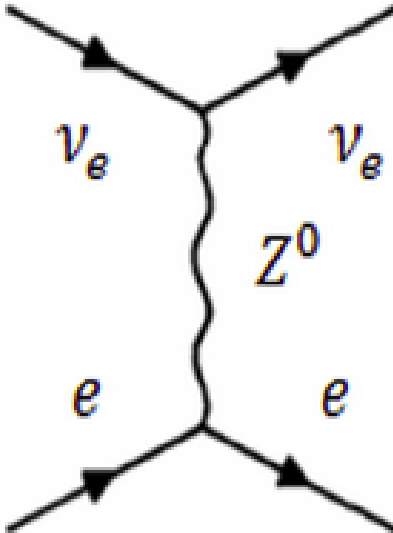

Figure 1.3: Feynman diagram of neutral current interaction

Since the mediator is chargeless, exchange of Z boson transfers momentum, spin and energy, but leaves the interacting particles' quantum numbers unaffected - charge, flavor, baryon number, etc.

$$l + \nu_l \rightarrow l + \nu_l$$

[l - lepton; ν_l - neutrino]

1.3.3 Matter effects

Normal matter contains a large number of e, but no μ or τ. While travelling through matter, electron neutrinos interact through both charged and neutral current pathways whereas muon and tau neutrinos interact only through neutral current pathway. As a result, electron neutrinos pick up an extra interaction term proportional to the density of electrons in matter. While calculating the matter effects on the probability of the oscillation, neutral current interactions are ignored as all neutrino flavours experience it equally. As a result of matter effects, the mixing angles will be different based on the media of propagation due to which the mixing matrix will be different than its vacuum counterpart.

When neutrinos pass through the earth, the earth is assumed to have a uniform density and the matter effects result in a change in oscillation probability. This is used in neutrino experiments, since the number of up-going and down-going neutrinos will be different, as mentioned earlier.

2   Detection of neutrinos

As neutrinos are hard to detect directly due to their weak interaction with matter, they are usually identified by the particles produced when they interact through charged/neutral interactions with heavy nuclei. The muon neutrino is the easiest to detect among the three flavour species. When the neutrino interacts with matter via charged interactions, they produce the corresponding charged lepton. The electron neutrino produces an electron, however it gives electromagnetic showers resulting in the energy being distributed among a large number of cascading electron/positron decays making it harder to detect. The tau neutrino produces a tau particle which is the heaviest lepton, so it easily decays to the lighter leptons, due to which it is hard to differentiate between the signal and the background decay products (e, μ). The muon neutrino produces a muon which gives clean hits, with occasional hadron showers which can be segregated.

2.1   Methods of detection

Generally, neutrino detectors are large so as to increase the number of neutrino interactions to gather a significant amount of events to analyse. Some detectors are also built underground to block out the background signals due to cosmic radiation which interfere with the main signal, i.e, the particles produced due to neutrino interactions. We will now look at various kinds of neutrino detectors.

2.1.1   Water Cerenkov

When a charged particle travels through a medium faster than the speed of light in that medium, it radiates a cone of photons known as Cerenkov light. This cone is aligned to the direction of motion of the particle and has an opening angle that depends on the velocity of the particle and the refractive index of the medium as shown in fig 2.1.

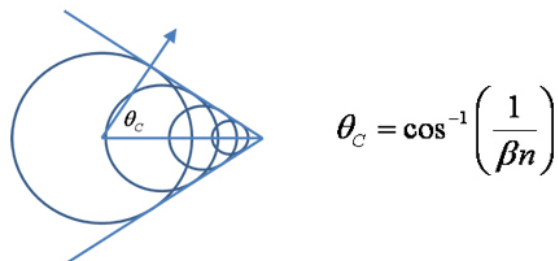$$\theta_C = \cos^{-1}\left(\frac{1}{\beta n}\right)$$

Figure 2.1: Cerenkov radiation

The target is surrounded by light sensors (Photo-Multiplier Tubes; detect light and converts it to an electric signal) which detects the cone as a circle of light. From the pattern of hits, the direction and energy of the particle can be reconstructed.
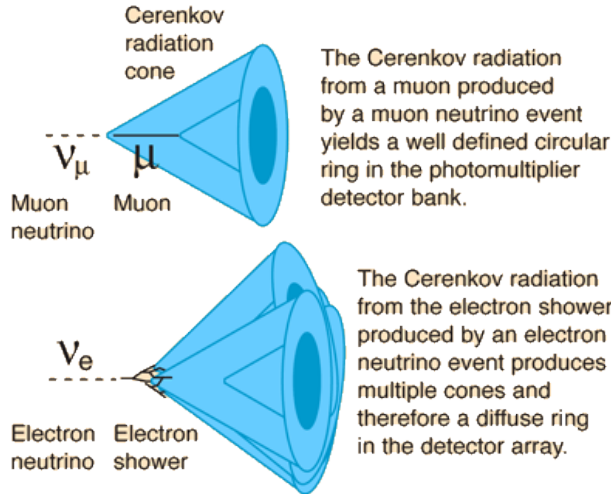
Figure 2.2: Cerenkov cones of muon and electron

However, particle identification is harder in cases like distinguishing a muon from a pion. It is possible to differentiate electromagnetic particles from muon-like particles by observing the shape of the ring outline. Electromagnetic particles tend to scatter in the target medium, leading to fuzzy rings, rather than the sharp edged rings seen with muon-like particles as shown in fig 2.2. Since the medium must be transparent and a large volume is required to gather enough events, water is the preferred medium for this setup. This is the detector setup in the Super Kamiokande experiment in Japan. Ice can also be used as a medium, like in the IceCube experiment in the South Pole.

The disadvantage with this type of detector is that is cannot detect neutral particles, or charged particles below the Cerenkov threshold. Moreover, if the number of particles increase, it becomes harder to reconstruct all the rings reliably. So, it is only suitable for particle decays involving few products and high energies.

2.1.2   Scintillation detectors

Scintillations are minute flashes of light which are produced by certain materials when they absorb radiation. It is a chemical process of luminescence, and generally the emission is of lower energy than the radiation. The threshold for scintillations is quite low, so it can be used for lower energy neutrino detection unlike cerenkov detectors. Scintillators can be either organic such as anthracene or inorganic crystals such as NaI, BaF_2, etc.

It works based on the same principle as water Cerenkov detectors. The scintillator is enclosed in a large volume and the inner walls of the volume are covered with photosensors to observe the scintillation light.
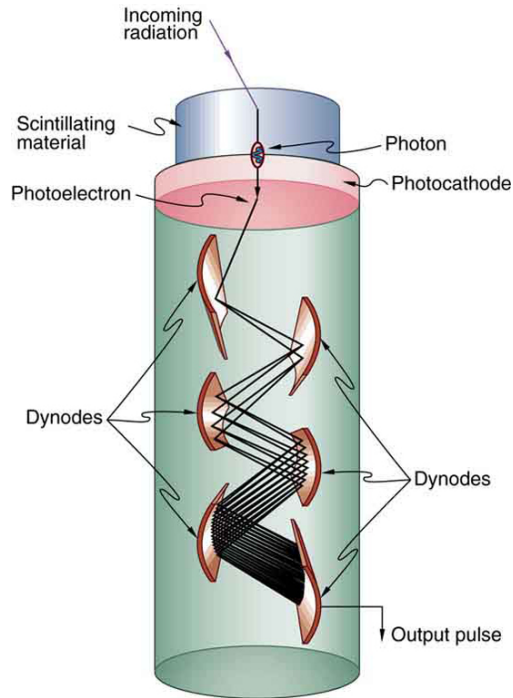
Figure 2.3: Scintillator detector setup

The intensity of the light pulse emitted by a scintillator is proportional to the energy of the absorbed radiation, so the latter can be determined by measuring the pulse height spectrum. There are multiple 'dynodes' in the Photomultiplier tube which basically serve as electrodes that multiply the number of electrons to amplify the signal. Such an arrangement is able to amplify the tiny current emitted by the photocathode, typically by a factor of one million.
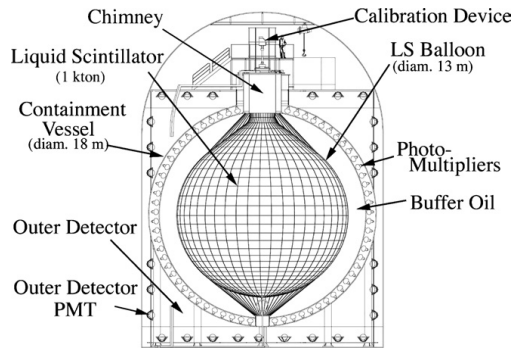

Figure 2.4: Schematic of KamLAND

Scintillator detectors are usually used to view electron antineutrinos being emitted from reactors. Neutrinos from reactors tend to have energies around 2-3 MeV. This is too low for water Cerenkov detectors, but visible to the scintillator detectors. However, since the scintillation light is isotropic (uniform in all directions), reconstruction of particle direction is not as good as the reconstruction in water Cerenkov. This setup is used in the KamLAND experiment.

2.1.3   Resistive Plate Chambers

Resistive Plate Chambers (RPC) are gaseous parallel plate detectors that are well suited for fast particle tracking of muons from muon neutrino interactions. These are used to track the position of the muon at various instants, and using this the momentum and direction of the muon are accurately reconstructed. This will be explained in section 3.
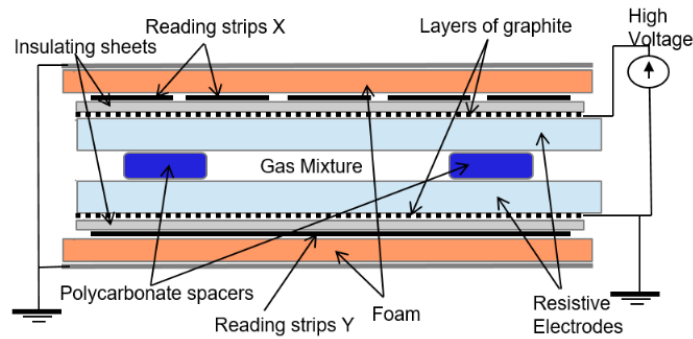
Figure 2.5: Sketch of a Resistive Plate Chamber (RPC) detector

An RPC consists of two parallel plates, made out of an insulating substance like glass or bakelite seperated by a gap of few millimetres. The whole structure is sealed airtight, with inlets and outlets to fill the space between the plates with a mixture of gases. The inner and outer surfaces are coated with graphite to provide electrodes and the outer surfaces have a row of parallel aluminium strips which are few cms wide from which the output is obtained. The aluminium strips on one surface are perpendicular to the strips on the other surface. A high voltage is applied across the two plates to polarize the gas molecules.
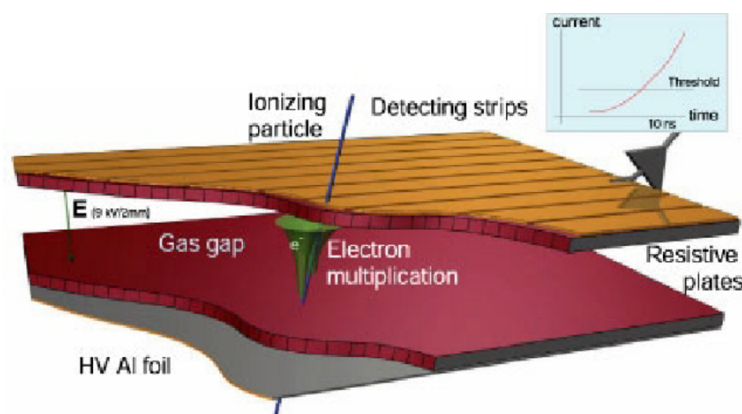
Figure 2.6: Cross section of RPC detector

There are two modes of operation based on the voltage applied and gas mixture used:

- **Streamer mode** In this mode, when the charged particle passes through the plates, continuous ionization occurs until there is a breakdown. The signal produced in this mode is in the order of a few hundred millivolts and does not require any amplification. Usually argon, SF6, isobutane and freons are used in the gas mixture for this mode.

- **Avalanche mode** When a charged particle passes through the plates, it ionizes the gas molecules in its path, and the produced ions further ionize the neighbour molecule, resulting in an 'avalanche' of positive and negative charges which get collected at either of the electrodes. Since the applied field opposes the induced one, the avalanche stops. This causes a signal current that is picked up by the aluminium strips on each surface. The pulse produced will be quite small, in the order of millivolts, and require amplifiers to read the signal.

Each strip is connected to a channel where the signal is fed to a Data Acquisiton system. The time delay in propagation of signal from the top and bottom surface of an RPC is adjusted by altering the lengths of the cable used to transfer the signal to the computer. Thus, an RPC provides a rough X and Y co-ordinate of a muon at some instant. By using layers of several RPCs, it is possible to reconstruct the trajectory and thereby the momentum and direction. Although streamer mode reduces cost as amplification is not necessary, it reduces the lifetime of the RPC, so the avalanche mode is the preferred mode of operation.

2.1.4 Tracking and Hybrid detectors

This is used in detecting high energy particles, where the neutrino energy is above a few GeV. In this case, the intention is to track each particle that is produced in the interaction. These detectors are a combination of active (realtime output) and passive (delayed output) detectors including the previously discussed cerenkov, scintillator and RPC detectors.The passive detectors quickly stop the particle to obtain an estimate of the momentum whereas the active detectors perform the actual detection to give position resolution of the particle. Particle energy is measured through three main routes, depending on particle type: range, magnetic tracking and shower calorimetry.
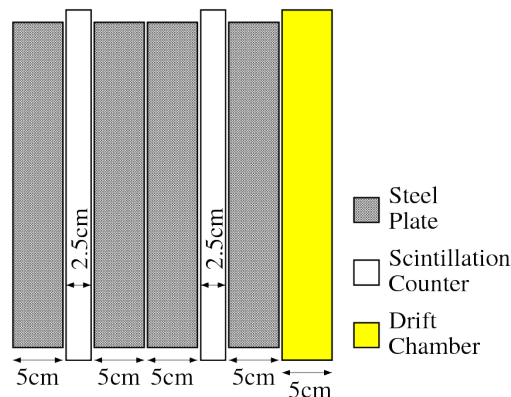
Figure 2.7: NuTeV detector setup

11

An example of this type of detector is NuTeV. NuTeV was a long detector composed of iron plates as the target, interspersed with scintillator and drift chambers for tracking. It was designed to look at high energy, deep inelastic scattering events.
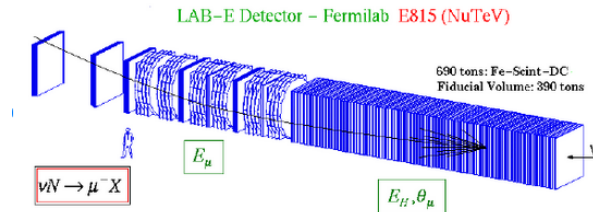

Figure 2.8: Sample NuTeV event

The first part of the detector provides a target for the neutrino beam and the second part forms a magnetic channel, which bends muons as they enter and provides momentum measurement. The hadronic part of the interaction interacts, and is contained in the iron. A sample event is shown in fig 2.8 showing the long muon bending as it goes through the magnetic channel, and the short hadronic shower splash near the vertex.

There are also other types of hybrid detectors that have fine-grained tracking, muon spectrometers, hardonic and electromagnetic calorimety and particle identification similar to the setup in the LHC. Thus, hybrid detectors use a combination of various detectors to give more accurate resolution of momentum and position of the paths of neutrino interactions, allowing us to study neutrino oscillations with much higher precision.

2.2   Detector efficiency

The efficiency of a detector must be taken into account while building it, and this depends on various factors depending on the kind of detector; RPCs for instance will have varying efficiency based on the gas composition used, and the width of pickup strips, etc. It can also depend on environmental variables such as temperature and humidity and location. For instance, cosmic muons may act as a background signal which can be reduced by situating the experiment underground. Detector efficiency can be studied based on two main features;

- **Spatial resolution:** This basically refers to the precision with which the detector can detect the position of the input signal; photons in case of cerenkov/scintillator and particle ionization in case of RPCs. The evaluation of the spatial resolution of a particle sensor involves irradiation of the sensor with particle beams at various energies and the measurement of the differences between the measured impact points with the real ones.

  For water cerenkovs, it might depend on the size, number and area coverage of the light sensors (PMT) around the volume. For RPCs, it might depend on the size of the plates, and the width and number of aluminium strips used.

- **Time resolution:** The time resolution is defined by how accurately the time at which a particle crossed the detector can be determined. This is important while reconstructing the tracks, specifically while determining the direction of the particle along the track.

There are also other resolutions that are important for neutrino detection, dependant on the kind of detector used, like energy and angular resolution for RPCs, however those are determined mostly through simulation data, and will be discussed in the upcoming sections.

3 Track reconstruction in RPCs

This section will look into the process of reconstructing muon tracks from the data obtained from stacks of RPCs wedged between iron plates (similar to the setup of the INO-ICAL experiment). The next section will deal with the ICAL detector geometry and a small simulation study of the detector performance.

As discussed earlier, each RPC provides a spatial co-ordinate for each time a muon passes through the detector. These co-ordinates are grouped together, classified, and reconstructed to roughly form the trajectory of the muon. Generally, a magnetic field is applied, due to which the trajectory is an arc and the momentum can be obtained from the parameters of the arc. An algorithm is used to obtain statistically accurate trajectories by combining the vast number of co-ordinates the RPCs have collected. The following sections will describe the process of reconstruction.

3.1 Track finding

Track finding involves reconstructing the trajectory from a purely geometric perspective. This section will show how the individual data points are identified, sorted and finally lead to track reconstruction.

3.1.1 Hits

As we know, RPCs give an X and Y co-ordinate whenever a muon passes through it, and the Z co-ordinate can be determined by the position of the RPC in the stack. An algorithm forms ordered pairs of co-ordinates if the difference in X and Y detection timing is less than 1 ns. Each set of co-ordinates caused by a muon detection and rebuilt by the algorithm is called a **'hit'**. Each hit is accompanied with a time stamp indicating roughly the time of detection (within errors of time resolution of the detector).

The Data Acquisition system filters out the hits to segregate the actual events from noise. The hit is basically an electric pulse which is relayed, and so the pulses with amplitude less than some treshold are removed from the dataset, and the pulse parameters of the qualified hits are discarded. Due to this, particle identification is a bit of a challenge since hadronic hits and leptonic hits can't be differentiated as the pulse information is not stored.

3.1.2 Clusters

Now, the hadronic hits must be identified and discarded to accurately reconstruct the muon trajectory. This is done by a robust algorithm. The basic idea is, if there are around 6 or more hits within a short period of time on the same RPC panel, all the hits on that level are discarded, since hadrons give hadronic showers and cause a lot of hits. Although few muon hits may be eliminated as well, it overall improves accuracy of the reconstruction. This kind of an algorithm is basically a 'Pattern recognition' software which could be based on Machine Learning techniques.

If there are 3 or more hits close to each other, they are classified as a single object called a 'cluster'. It is possible that a single muon caused signal pulses on multiple pickup strips, so sorting a cluster as a single object takes care of those scenarios.
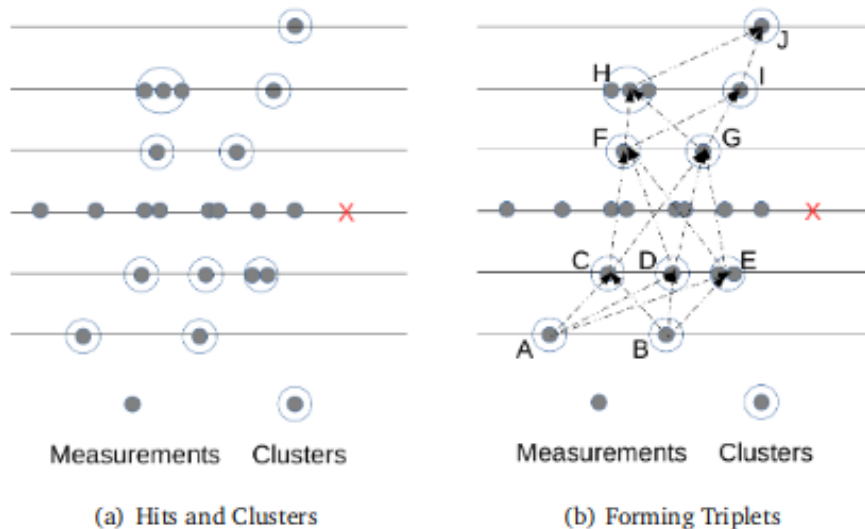
3.1.3 Triplets

Figure 3.1: Formation of (a) Hits and Clusters (b) Triplets

The clusters and hits are then coupled in various ways to form 'triplets'. This is done by calculating the slope between every two points, and sorting the points in 3 consecutive layers having the difference in slope less than a certain value (depending on the applied magnetic field) into a **'triplet'**. This triplet forms a segment of the full trajectory, and decreases the amount of data to be handled while preserving the information. These triplets are stored under a 'tracksegment' class object.

3.1.4 Track segments

The triplets are now matched with each other to form a chain of triplets. A random triplet is selected, and other triplets are attached to it, based on their compatibility to form a track

segment. This track gets longer as more triplets are appended to it. Multiple such segments are constructed over recurring iterations till all the triplets have been utilized as part of a track. There are three possible cases that may arise while associating triplets:

- **Case 1: Z co-ordinate of end of first segment is greater than second segment**
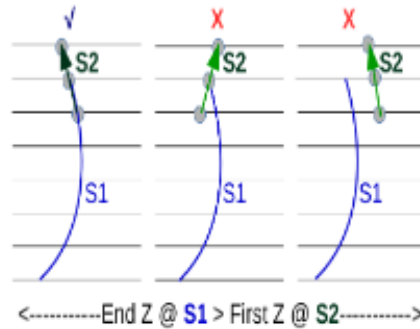

Figure 3.2:

In this case, if overlapping of few clusters of both segments is observed, triplet S2 gets appended to the S1 track segment.

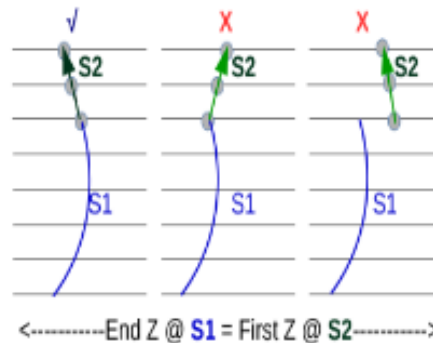- **Case 2: Z co-ordinate of end of first segment is same as that of second segment**

Figure 3.3

In this case, two conditions are checked; Firstly, the last cluster of both segments must be the same one and secondly, the slope at the end of first segment is almost same as the slope of the end of the second segment as shown in fig 3.3.

- **Case 3: Z co-ordinate of end of first segment is lesser than second segment**
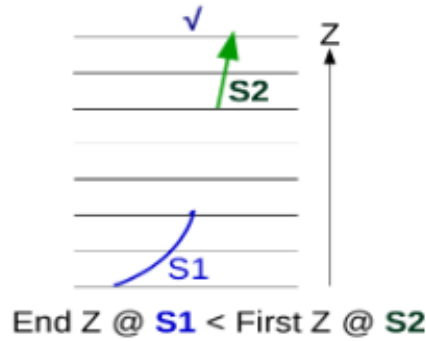

End Z @ **S1** < First Z @ **S2**

Figure 3.4

In this case, there will be a portion of the track where we have no data about the trajectory. It is possible that the particle may have passed through a blind spot of the detector leading to no hits recorded in that region. If the slopes of the two segments are not very different, they are appended onto the same track.

In fig 3.2, 3.3 and 3.4, S1 is the existing chain of triplets, and S2 is the new 'test' triplet to be appended. Once the chain of triplets has more than 5 clusters/hits, it forms a **track**.
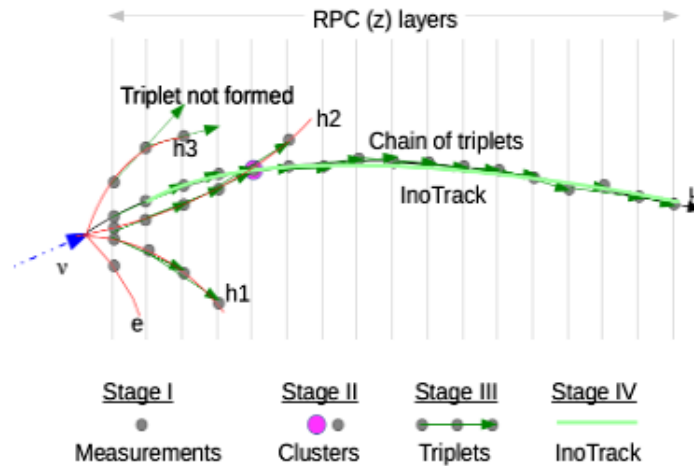
3.1.5 Forming Tracks

Figure 3.5: Muon track and Hadron shower

Once multiple track segments have been formed, they are further appended to create the tracks. If there are two or more tracks, the longer track is taken as the muon track and the left over hits, clusters, triplets and segments are taken to be formed by π^-, e^-, p^+. These unused parts form the hadron shower.

16

3.2   Track Fitting

After track finding, track fitting is done to obtain the parameters of the muon track and thereby, information about the incident neutrino/anti-neutrino. During track finding, the hits are processed from a geometric perspective. But for track fitting, the effects of motion of the particle through the detector is also taken into account, like energy loss, coulomb scattering, etc. Using the tracks formed from track finding as a seed, the algorithms fits the track to a model to obtain the optimal set of track parameters that explains the experimental data. A recursive least square fitting technique called Kalman filter is used to work with all this data.

A Kalman-filter based algorithm is used to fit the tracks based on their curvature due to the magnetic field. Every track is identified by a starting vector $X_o = (x, y, dx/dz, dy/dz, q/p)$ which contains the position of the earliest hit as recorded by the track finder, with q/p taken to be zero. To start the fitting, few properties of the track are required:

- **Z-direction:** The direction of a muon is determined from the time data of the clusters. If T(Z) denotes the set of timing data measured along different Z coordinates of the clusters along the track, then the first derivative of T(Z) determines direction.

$$\frac{dT}{dZ} = \frac{n \sum_{i=1}^{n} Z_i T_i - \sum_{i=1}^{n} Z_i \sum_{i=1}^{n} T_i}{n \sum_{i=1}^{n} Z_i^2 - (\sum_{i=1}^{n} Z_i)^2}$$

- **Vertex Position:** Usually, a pattern recognition software is employed to find the cluster closest to the vertex. So, the position of this cluster belonging to the formed track is taken as the vertex position of the seed track.

- **Calculating X and Y slopes:** The values of dX/dZ and dY/dZ near the initial point is required. The clusters in the neighbouring Z planes are used to calculate the slopes locally(for point on i^{th} Z plane, calculation is done from $(i-2)^{th}$ plane to $(i+2)^{th}$ plane).

$$t_A = \frac{dA}{dZ} = \frac{n \sum_{i=1}^{n} Z_i A_i - \sum_{i=1}^{n} Z_i \sum_{i=1}^{n} A_i}{n \sum_{i=1}^{n} Z_i^2 - (\sum_{i=1}^{n} Z_i)^2}; \quad A = (X, Y)$$

- **Fully and Partially contained events:** The muon track may be fully or partially contained within the RPC stack, and these tracks must be separated. The tracks that have max/min Z-coordinate within two layers from top/bottom Z boundaries of the stack are taken to be partially contained. Also, if the X/Y coordinate at the end of the track extrapolated through 2 more Z layers gives a point outside the boundary, it is also taken to be partially contained. All other events are fully contained.

- **Events in blind spots:** At the boundaries of the RPCs, if muon passes through these points they cannot be detected, and the length they traverse without detection cannot be determined. These events must be separated, otherwise it results in the estimated momentum turning out to be lesser than it should be due to which the accuracy of momentum estimation becomes worse.

In track fitting, a theoretical model of evolution of the initial vector is constructed. This model extrapolates the state to future measurement sites. So, a χ^2 is calculated between the prediction and the measurement, and this value is minimized to obtain the track parameters like initial momentum and direction of the muon.

3.3   Reconstruction efficiency

The performance of the program depends on how well it has reconstructed the track parameters, compared to the actual trajectory of the muon. The efficiency of the algorithm is validated by checking the following parameters. These are usually run in simulations to gather data before implementing it in experiments.

3.3.1   Particle Identification

The ability to seperate the hits due to muons from the hits due to hadrons. Since reconstruction is a statistical process, it is likely that the algorithm identifies a hadron event as a muon one or fails to identify an actual muon event. From a simulation run, the ratio of correctly identified hits and the total hits, as well as number of incorrectly rejected hits are calculated to find out the efficiency of particle identification.

3.3.2   Direction and momentum reconstruction

Identifying the direction of the muon track is important to deduce whether it was from a neutrino or an anti-neutrino. So, the up-down efficiency is noted as the fraction of incorrectly identified events to the total number of events. This can depend on the input momenta as well as direction, since its harder to determine direction of a nearly horizontal track. Similarly, the momentum reconstruction efficiency is defined as the ratio of number of recontructed events(n_{rec}) to the total number of generated events, N_{total}.

$$\epsilon_{rec} = \frac{n_{rec}}{N_{total}}$$

and its error, $\delta\epsilon_{rec} = \sqrt{\epsilon_{rec}(1 - \epsilon_{rec})/N_{total}}$

3.3.3   Relative charge identification

The charge identification of the particle distinguishes neutrinos from anti-neutrinos and so is an important quantity to identify correctly. Relative charge identification efficiency is defined as the ratio of number of events with correct charge identification, n_{cid}, to the total number of reconstructed events;

$$\epsilon_{rec} = \frac{n_{cid}}{n_{rec}}$$

and its error, $\delta\epsilon_{cid} = \sqrt{\epsilon_{cid}(1 - \epsilon_{cid})/n_{rec}}$

3.3.4 Momentum and angular resolution

After track fitting, the algorithm determines the momentum and initial angle of entry of the muon among other track parameters. The resolution, i.e, accuracy of momentum and zenith angle recontruction depends both on the detector itself and the pattern recognition algorithm.

$$P_{res} = \frac{\sigma}{P_{in}} \ ; \quad \frac{\delta P_{res}}{P_{res}} = \frac{\delta \sigma}{\sigma}; \quad \theta_{res} = \sigma$$

4 Simulation study of INO-ICAL events

4.1 India-based Neutrino Observatory

The India-based Neutrino Observatory (INO) is a proposed underground laboratory to be built in Tamil Nadu. Few of the experiments to be conducted at INO are:

- the Iron CALorimeter (ICAL), to observe neutrino oscillations

- the Neutrino-less Double Beta Decay (NDBD) experiment, to verify properties about neutrinos and anti-neutrinos

- the Dark matter search in INO (DINO) experiement

The ICAL detector is a 50kton magnetized iron calorimeter, built to observe atmospheric neutrinos. It will attempt to resolve the mass heirarchy problem by observing neutrino oscillations. It detects the muon tracks due to muon neutrinos, and has the ability to find the charge, momentum and direction of the muons. This data can be used to deduce the ratio of neutrino/anti-neutrino at various energy levels. To reduce the background cosmic muons, the laboratory is planned to be built underground, within a cavern beneath the west Bodi Hills, near Theni in south India. Most of the muons are absorbed by the surrounding rocks.
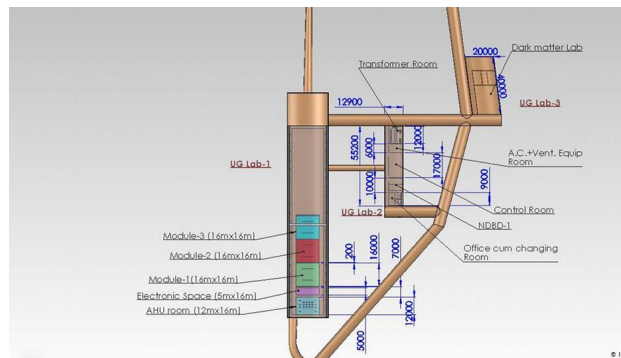

Figure 4.1: India-based Neutrino Observatory(INO) Schematic

Besides trying to solve the mass heirarchy, INO also plans to measure oscillation parameters more accurately. The ICAL experiment is in R&D stage, and will be followed by planning two other experiments in the future; NDBD and DINO.

4.1.1   Iron Calorimeter
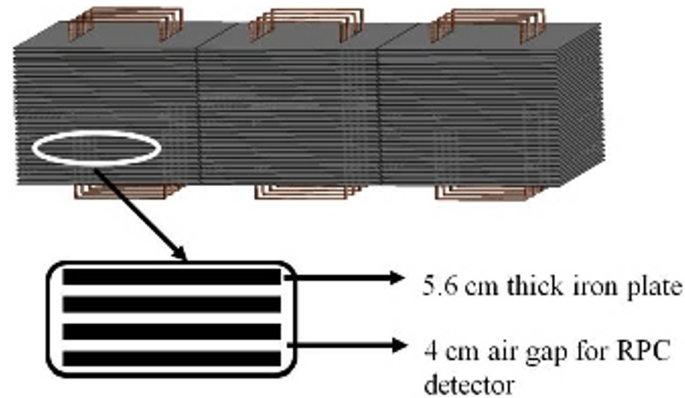
- **Detector Geometry**

Figure 4.2: Schematic of ICAL detector

The ICAL detector will use 50 kton of iron plates as passive elements and glass resistive plate chamber (RPC) detectors as active elements. A total of 150 layers of RPCs are sandwiched between 151 layers of iron plates, each of thickness 5.6 cm. Between each successive iron plate, there is a 4cm gap to place an RPC. The complete detector dimensions are 48m x 16m x 14.5m. The detector is divided into three modules, each with dimension 16m x 16m x 14.5m. This modularity is introduced so that one module can gather data while the other modules are being constructed. Iron is chosen as the target material due to its high density, and good magnetic properties. Glass RPCs are preferred than Bakelite RPCs or scintillator setups due to lower costs.

(a) Detector geometry
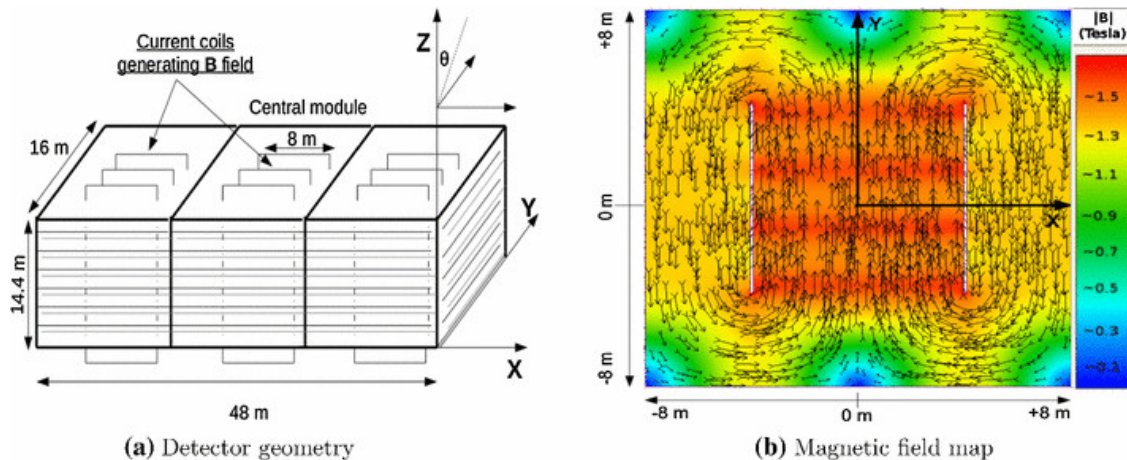
(b) Magnetic field map

Figure 4.3

Each RPC has 2mx2m dimension, so each layer in a module has 64 RPCs. There are also iron spacers supporting each layer, located every 2m along x-direction. This

creates 2m wide channels along y-direction for placing RPCs. The whole setup will be surrounded by scintillation detectors which act as a screening layer to identify muons entering from outside the detector.

Each module of ICAL is equipped with four current carrying coils, having 60kA current to magnetize the core to 1.5T. This magnetic field helps in recognizing neutrinos from antineutrinos as their secondary particle curve in different directions.

4.2   Simulation study

Before implementing an experiment, simulations are run to obtain sample data to test the performance of the apparatus and its sensitivity to various parameters. In this section, we will discuss an analysis of the INO-ICAL detector efficiency with simulated data.

Firstly, a large number of muon events are generated (in this case 10,000 events) in a software like NUANCE/Pythia, and then the detector geometry is modeled in GEANT4. The muon events are then simulated in the GEANT4 detector environment to generate hits on the detectors. The track parameters are then reconstructed using pattern recognition and filter algorithms and we obtain a set of values such as the reconstructed momenta, reconstructed positions, energy measured in the calorimeter, etc in a ROOT file.
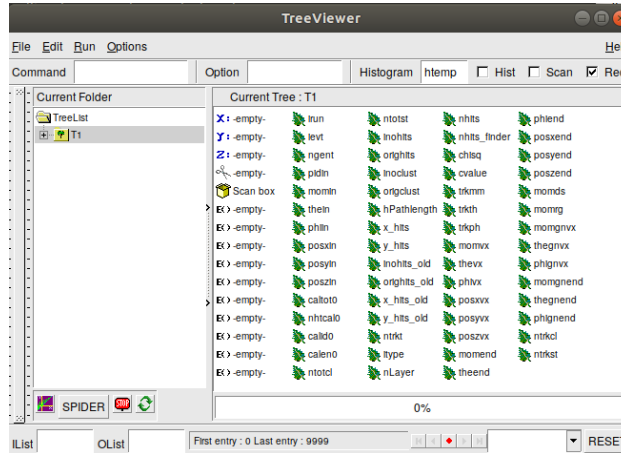

Figure 4.4: Output data from simulations

In this analysis, 56 data files have been used with varying parameters;

- **Initial momentum:** 1-12 GeV/c, 15 GeV/c, 20 GeV/c

- **Initial zenith angle:** 0.4547 rad, 0.7853 rad, 0.6074 rad, 0.3154 rad

The initial position of the muons are (100,100,0), with the center of the module being the origin (0,0,0). The azimuthal angle of the muons are uniformly random and the output values we use in this analysis are reconstructed momentum and reconstructed zenith angle.

4.2.1 Zenith angle resolution

The reconstructed zenith angle distribution is plotted and fit to a gaussian. The sigma of the gaussian is the resolution of the angle which indicates the accuracy of measurement of the zenith angle.
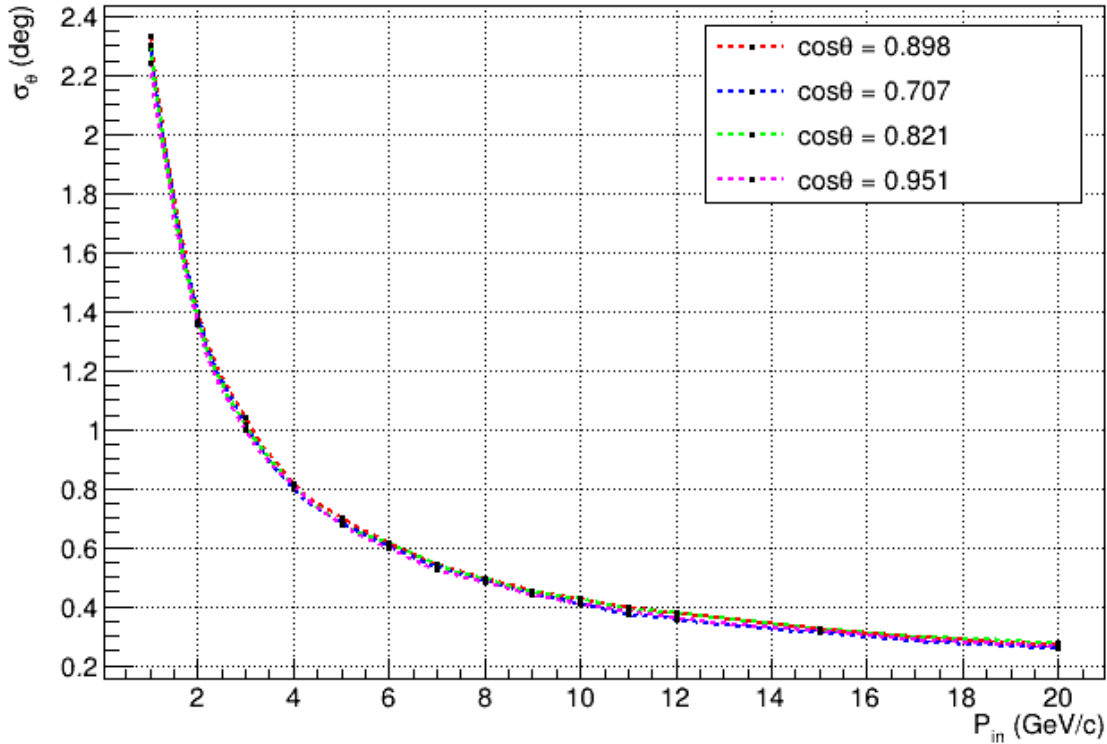

Figure 4.5: Zenith angle resolution

The angular resolution was plotted for different (P_{in}, θ_{in}) pairs, and as we can see, it has an inverse dependancy on the input momentum, however is nearly independant of the zenith angle itself.

4.2.2 Momentum resolution

When the reconstruction momentum distribution is fitted with a gaussian, we can see that the χ^2/ndf is around 10, and the histogram does not exactly fit a gaussian. This is because, the resolution of momentum varies for different azimuthal angles, since the mean and the width of the four azimuthal bins vary. This could be because the magnetic field has slightly different effects at the edges and at the center (as it is produced by current carrying coils).
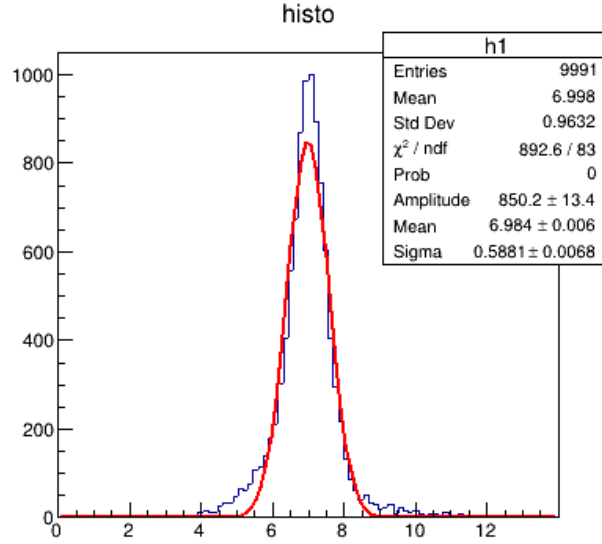
Figure 4.6: Momentum distribution of (7 GeV, 0.4547 rad)

However, if we divide the plot into four parts based on the azimuthal angle of the muon; (a) $0 < |\phi| \leq \frac{\pi}{4}$; (b) $\frac{\pi}{4} < |\phi| \leq \frac{\pi}{2}$; (c) $\frac{\pi}{2} < |\phi| \leq \frac{3\pi}{4}$; (d) $\frac{3\pi}{4} < |\phi| \leq \pi$ The distribution fit the gaussian much better, with χ^2/ndf getting closer to one.
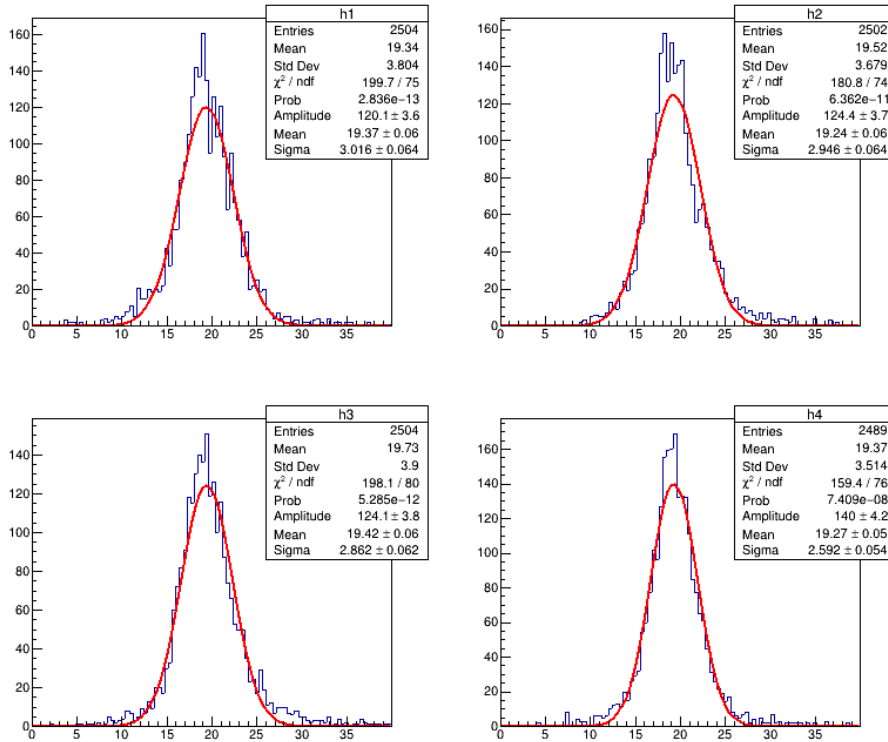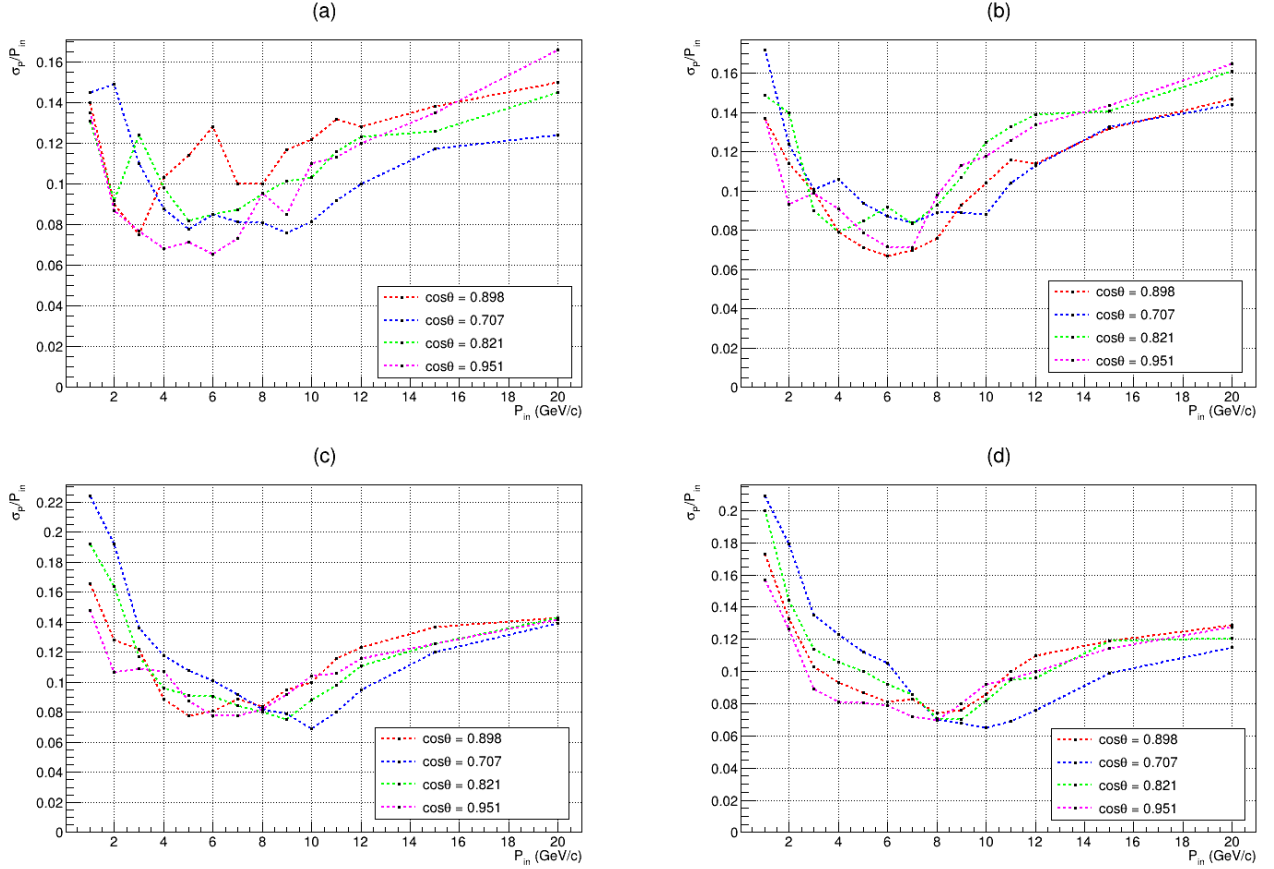

Figure 4.7: Momentum distribution after seperating into azimuthal bins
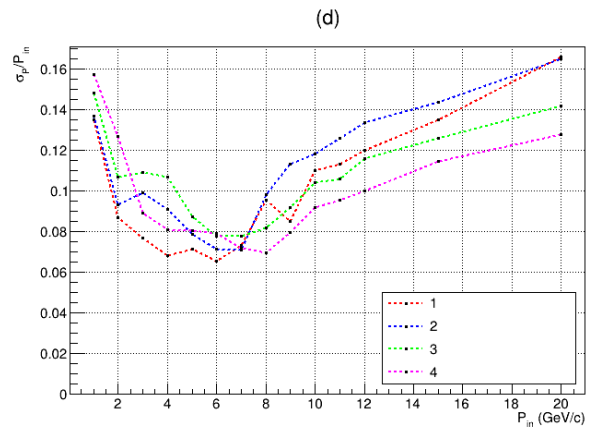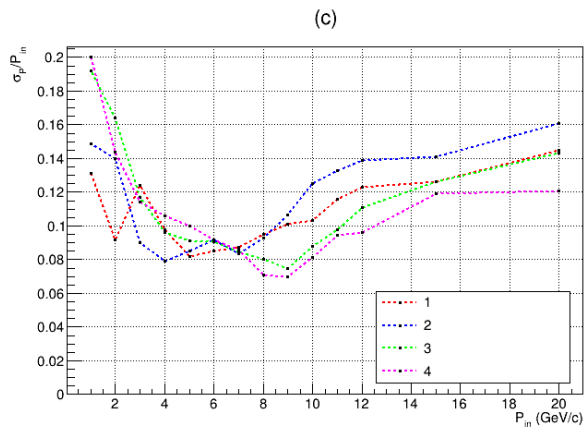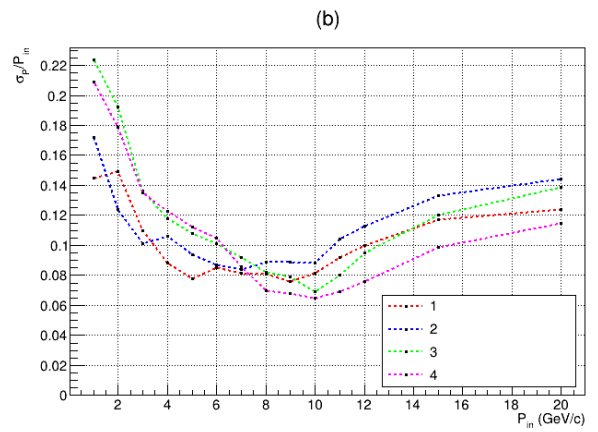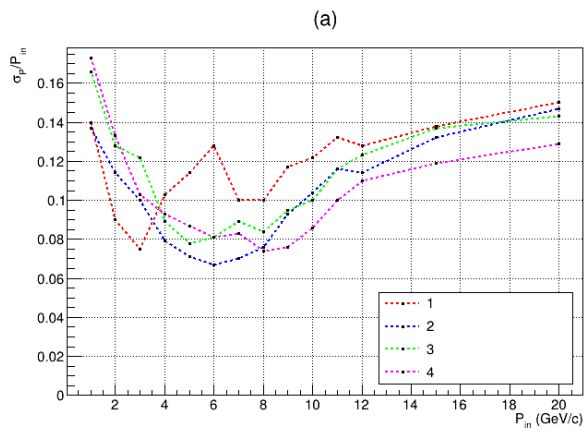
Table 1: Muon resolution in four quadrants:
(a) $0 < |\phi| \leq \frac{\pi}{4}$; (b) $\frac{\pi}{4} < |\phi| \leq \frac{\pi}{2}$; (c) $\frac{\pi}{2} < |\phi| \leq \frac{3\pi}{4}$; (d) $\frac{3\pi}{4} < |\phi| \leq \pi$

Initially, upto 6 GeV, the resolution improves with increasing energy, since the muons tend to travel through more RPC layers and generates more hits, so the reconstruction algorithm has better efficiency. However, as the momentum increases further, the particle begins exiting the detector resulting in partial tracks that would be almost straight sections, since the magnetic field results in a larger radius of curvature. This results in loss of resolution (higher momentum resolution value). This roughly agrees with the graphical representation of the data in Table 1. The dependency of resolution on the input momentum, is however, quite erratic for the first azimuthal bin.

Table 2 shows the distribution in each azimuthal angle bin for the different initial zenith angles. We can see that, for all four zenith angles, the momentum resolution at higher energies is roughly highest(best) for $\frac{3\pi}{4} < |\phi| \leq \pi$, and is lowest for $\frac{\pi}{4} < |\phi| \leq \frac{\pi}{2}$.

Table 2: Muon resolution for different $cos\theta$ seperated in azimuthal bins:
(a) $cos\theta = 0.898$; (b) $cos\theta = 0.707$; (c) $cos\theta = 0.821$; (d) $cos\theta = 0.951$

4.2.3 Mean shift of reconstructed momentum

The reconstructed momentum distribution is fit to a gaussian. For input momentum P_{in} and mean momentum from the gaussian P_{rec}, the mean shift is $P_{in} - P_{rec}$.
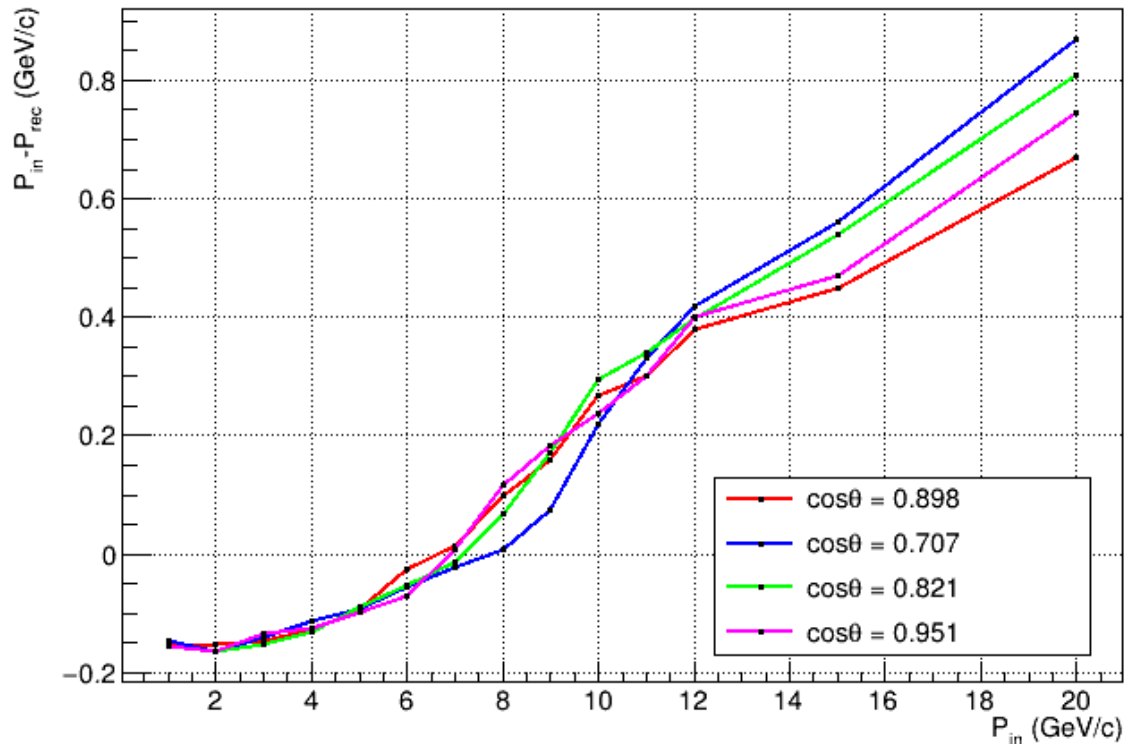

Figure 4.8: Mean shift of reconstructed momentum

Below 6 GeV/c momentum, the mean shift is negative, after which it turns positive and peaks at 0.8 GeV/c. Till 12 GeV/c, the mean shift is roughly independant of zenith angle, however after that point, it shows a weak dependancy for higher initial momenta. The shift can arise due to multiple scattering, etc., and is roughly linear beyond a few GeV/c.

4.2.4 Reconstruction efficiency

Again, the reconstructed momentum distribution is fit with a gaussian. The integral of the gaussian is then computed within a 3σ range of the mean, and the ratio of this integral and the integral of the momentum distribution gives the efficiency, ϵ.
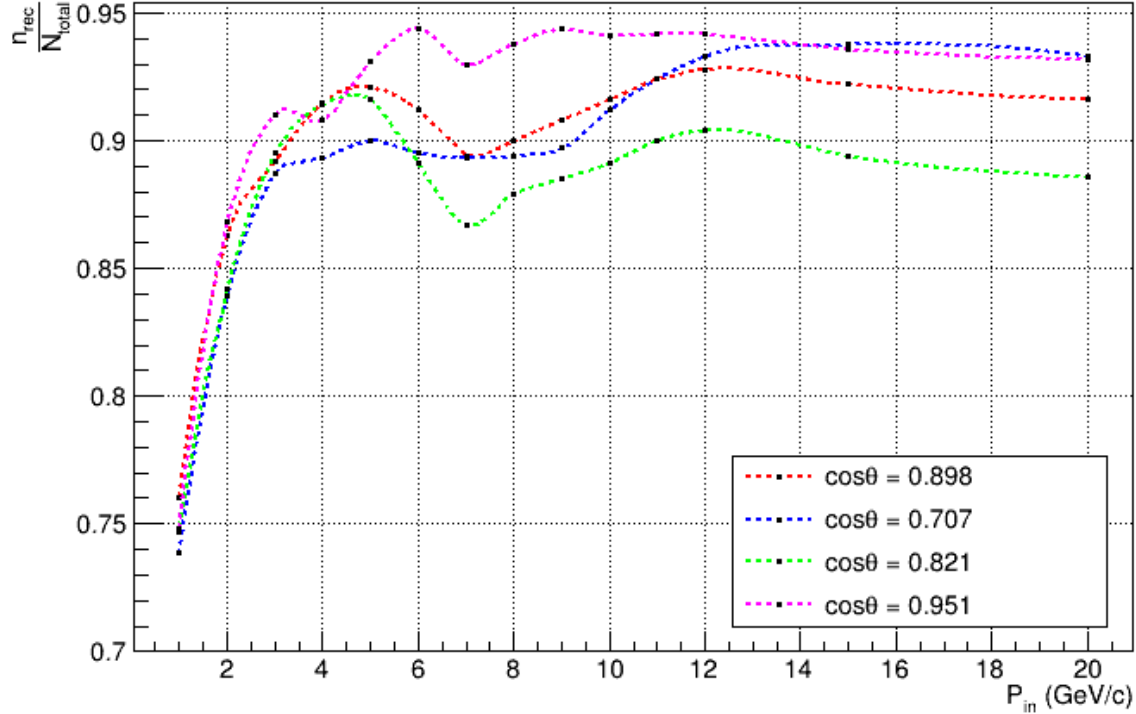

Figure 4.9: Reconstruction efficiency

The efficiency is low (¡90%) for $P_{in} < 4$ GeV/c, after which it reaches a peak, drops again at 8 GeV/c and rises up to even out at the higher momenta. We can also see there is a clear dependancy on zenith angle, as the $\cos\theta$ =0.821 curve reaches the lowest maximum efficiency, and the $\cos\theta = 0.951$ curve reaches the highest maximum efficiency. Below 4 GeV/c, the efficiency is low since the number of hits due to low energy muons are lesser, so the reconstruction algorithm has lesser hits to form the tracks. However, the efficiency steadily increases since the number of hits increases with input momentum. After 4 GeV/c, the efficiency dips, because the tracks become nearly linear (since $R = \frac{mv}{Bq}$, radius increases with momentum) due to which, momentum reconstruction becomes harder. At higher energies ($P_{in} > 12$ GeV/c) the efficiency becomes constant.

5   Conclusion

Neutrino oscillation continues to be one of the major areas of research in particle physics, and the detection methods discussed (cerenkov tanks, scintillators, RPCs, etc) are being employed in various long-baseline neutrino experiments to accurately determine the oscillation parameters and solve the problem of mass heirarchy. The ICAL detector in INO is proposed for this purpose and has RPCs as it's active detector element.

The simulation analysis performed in section 4 was done in ROOT and the following results were observed;

- The angular resolution of the detector is very good, at less than 1 degree for momenta larger than 3 GeV/c and is independant of the zenith angle.

- The momentum resolution of the detector as a whole is not good, however when seperated into azimuthal bins, the resolution ranges from 6-20% based on the zenith angle and initial momentum. The shape of the resolution plot also matches with the logical interpretation of the behaviour of the muon track in the specified detector geometry.

- The reconstruction efficiency ranges from 75%-95% and becomes nearly constant for higher momenta. So, muon neutrinos with initial momentum $> 4GeV$ are detected with better accuracy (within a 3σ error bound) and provides satisfactory results.

Overall, the simulations suggest that the detector has fairly good response to muons, and the algorithm can reconstruct tracks with good efficiency. The momentum and angle resolutions have been checked, however the charge identification efficiency has not been determined in this analysis. Moreover, the variety of zenith angles used here do not cover all possible cases, so the results obtained are partial evidence to the good response of the detector. Further analysis is to be done to obtain a better understanding of the ICAL detector efficiency.

6 References

[1] https://link.springer.com/content/pdf/10.1140%2Fepjc%2Fs10052-019-6798-0.pdf

[2] http://t2k-experiment.org/neutrinos/neutrino-detection/

[3] http://www.ino.tifr.res.in/ino/theses/2015/Thesis_Kolahal.pdf

[4] http://inspirehep.net/record/1444551/files/tapasi_thesis.pdf

[5] http://inspirehep.net/record/1621606/plots

[6] https://warwick.ac.uk/fac/sci/physics/staff/academic/boyd/stuff/neutrinolectures/lec_-neutrinodetectors_writeup.pdf

[7] http://www.ino.tifr.res.in/bsn/INO/Mathi%20RPC%20report1.pdf

[8] http://meroli.web.cern.ch/Lecture_SpatialResolution.html

[9] http://www.tifr.res.in/ gobinda/inosim/anal_inoical.C

[10] https://arxiv.org/pdf/1405.7243.pdf